This is a repository copy of *Dynein structure and power stroke* .

White Rose Research Online URL for this paper:
http://eprints.whiterose.ac.uk/116/

Article:

Dynein structure and power stroke

Stan A. Burgess*, **Matt L. Walker***, **Hitoshi Sakakibara**†, **Peter J. Knight*** & **Kazuhiro Oiwa**†

* *Astbury Centre for Structural Molecular Biology & School of Biomedical Sciences, University of Leeds, Leeds, LS2 9JT, UK*
† *Kansai Advanced Research Centre, Communications Research Laboratory, Kobe, 651-2492, Japan*

....

Dynein ATPases are microtubule motors that are critical to diverse processes such as vesicle transport and the beating of sperm tails; however, their mechanism of force generation is unknown. Each dynein comprises a head, from which a stalk and a stem emerge. Here we use electron microscopy and image processing to reveal new structural details of dynein c, an isoform from *Chlamydomonas reinhardtii* flagella, at the start and end of its power stroke. Both stem and stalk are flexible, and the stem connects to the head by means of a linker approximately 10 nm long that we propose lies across the head. With both ADP and vanadate bound, the stem and stalk emerge from the head 10 nm apart. However, without nucleotide they emerge much closer together owing to a change in linker orientation, and the coiled-coil stalk becomes stiffer. The net result is a shortening of the molecule coupled to an approximately 15-nm displacement of the tip of the stalk. These changes indicate a mechanism for the dynein power stroke.

Dyneins fall into two principal classes[1]. Isoforms in the $9 + 2$ axoneme produce the propagating bending motions of cilia and flagella[2–5]. Cytoplasmic isoforms drive a variety of fundamental cellular processes, including nuclear migration, organization of the mitotic spindle, chromosome separation during mitosis, and the positioning and function of many intracellular organelles[6]. Each dynein is a complex of between 1 and 3 heavy chains, each with a relative molecular mass greater than 500,000, together with a number of intermediate and light chains[7]. Each heavy chain contains the sites of ATP hydrolysis and microtubule binding, and thus constitutes the fundamental motor unit[8]. Electron microscopy has established that the heavy chain folds to form a globular head with two elongated structures, the stalk and stem, emerging from it[9–11]. These two structures bind the microtubule track and cargo, respectively[7,12,13]. The stalk is up to 15 nm in length in some species[10] and is most probably an anti-parallel coiled-coil[14]. A small globular domain at its tip is the ATP-sensitive microtubule-binding domain[14–16]. The stalk and head are formed by the carboxyterminal two-thirds of the heavy chain[14,17]. The stem, which also binds the intermediate and light chains[7], is formed by the aminoterminal region and contains numerous short stretches with predicted coiled-coil structure[18,19].

Dyneins are AAA proteins

Dynein heavy chains belong to the AAA superfamily of mechano-enzymes (ATPases associated with diverse cellular activities)[20], each containing six tandemly linked AAA modules within the head[12,13,21]. Electron microscopy studies have indicated that the head is a ring-like arrangement of domains[17], consistent with the finding that other members of the AAA superfamily form ring-like structures[21]. Only four of the dynein AAA modules (numbers 1–4) have conserved P-loop signatures[18,19], compatible with functional nucleotide binding at these sites[22]. However, AAA1, nearest the N terminus, is the only one that hydrolyses ATP at an appreciable rate[23]. The function of the remaining three sites is unknown but they are thought to act in a regulatory role. This is most probably mediated by binding ADP, as, for some dyneins, ATP-induced microtubule translocation *in vitro* either requires ADP or is accelerated by it[24,25].

In the cycle of ATP hydrolysis, release of ADP and phosphate (Pi) from dynein is associated with the power stroke[26]. In the presence of ATP and vanadate (Vi), dynein forms a stable complex (ADP•Vi-dynein), thought to mimic the ADP•Pi state and hence the pre-power-stroke conformation of the motor[26]. Its structure in the absence of nucleotide (apo-dynein) is thought to represent the post-power-stroke conformation[26]. Electron microscope studies of

the outer-arm dynein complex *in situ* have shown that these two biochemical states have distinct conformations[27,28], and both have been found in motile flagella in the presence of ATP, establishing that they exist within the chemo-mechanical cycle of dynein[28]. Thus, the transition from ADP•Vi states to apo-states is analogous to product release and the power stroke. However, each outer-arm complex comprises multiple dynein heavy chains that were not resolved in these structural studies, so the conformational change in an individual heavy chain remains unknown. The existing evidence suggests that the mechanism of dynein is likely to be different from those of the other, much smaller, linear motors kinesin and myosin[29]. However, it remains unknown which part of the molecule amplifies the conformational change within the active site in the head into large-scale movement, and how the coiled-coil stalk conveys conformational changes to the ATP-sensitive microtubule-binding domain at the tip of the stalk.

Dynein c structure at the start and end of the power stroke

Figure 1 shows isolated molecules of a monomeric, flagellar, inner-arm dynein (subspecies c) imaged in both biochemical states using negative stain. These images show that the ADP•Vi molecule has the same general form as the apo-molecule[10,30], but the latter is more compact. We have used single-particle image processing[31] to reveal this change more clearly. Dynein c adopts two characteristic orientations on the carbon support film, providing two views (left and right) related by a roughly 180° rotation about the long axis of the molecule (Fig. 2a–h). Flexibility within the molecule produces a
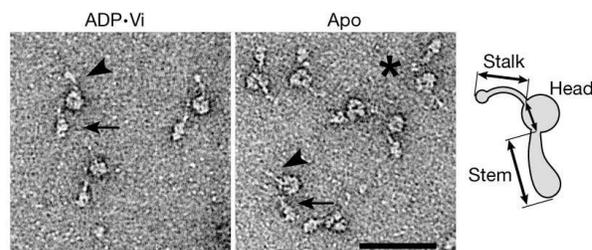
Figure 1 Negatively stained molecules of ADP•Vi-dynein c (left panel) and apo-dynein c (middle panel) from *C. reinhardtii* flagella. The preparation is monodisperse. Stems (arrows) and stalks (arrowheads) are indicated. The asterisk shows a molecule with a longer stem (see Fig. 2i). Scale bar, 50 nm. The right panel is a diagram of dynein c defining the stem and stalk, and the separation between their emergence points from the head.

 715

continuous range of conformations of the stem and stalk (see Supplementary movies 1–4; see also http://www.leeds.ac.uk/bms/research/muscle/dynein) causing most of the relatively smaller stalk to become smeared out in these averages (Fig. 2a, b, e, f). In both biochemical states the stem most commonly emerges from the left side of the head (Fig. 2a, e). At its base the stem is wide, narrowing to a flexible neck about 2 nm wide and about 8 nm long, which bends sharply very close to the head. A second alignment, using just the part of each image containing the head, reveals head details optimally (Fig. 2c, d, g, h). These show that left views of the head are not mirror images of right views in either biochemical state, indicating that the two faces of the head are different.

Comparisons between ADP•Vi- and apo-molecules reveal a pronounced conformational change within the head region. In left views the ADP•Vi head is roughly circular (Fig. 2c), with a diameter of approximately 13 nm, whereas the apo-head has a markedly different shape and a prominent central stain deposit (Fig. 2g). Small variations in stain accumulation or viewing angle produce subtle differences in appearance between individual heads, which limit the detail in these global averages. Further classification of left views therefore reveals additional detail of the conformational change (Fig. 3a, b). A central stain deposit occasionally visible in ADP•Vi heads (Fig. 3a) has greater prominence in apo-heads (Fig. 3b). A similar difference is also apparent in right views (Fig. 2d, h). These observations suggest an opening or unblocking of a stain-filled channel. Right views also show three distinct domains arranged around one edge of the apo-head (asterisks), not seen in the ADP•Vi head, indicating that changes also occur around the periphery.

Movement of the stem

The most marked change in the molecule between different states is that stem and stalk are closer together in apo-molecules than in ADP•Vi molecules (compare Fig. 2g, h with c, d). The separation between their emergence points from the head in left views changes by 6.3 nm (mean chord length: ADP•Vi = 9.9 ± 1.3 nm (s.d.), $n = 1,235$; apo = 3.6 ± 0.9 nm, $n = 1,221$; measured as in Fig. 1 diagram). As there is little change in length of either the stalk

(mean chord length: ADP•Vi = 15.4 ± 0.9 nm, $n = 908$; apo = 15.5 ± 1.0 nm, $n = 721$) or the stem (ADP•Vi = 26.4 ± 1.2 nm, $n = 1,351$; apo = 25.0 ± 1.0 nm, $n = 1,351$; see Fig. 1 diagram) the origin of this change must be a translational movement between these two domains. This also brings the neck and head into closer proximity (for example, compare Fig. 3e with Fig. 3f) but has little effect on the distribution of stem chord angles (standard deviation in ADP•Vi = $18°$, $n = 1,351$; apo = $16°$, $n = 1,351$). A fine, tapering structure on the head (Fig. 3a, b, white arrows) provides a landmark, relative to which the emergence point of the stem clearly changes (Fig. 3a, b, black arrows), but the stalk does not. Thus the origin of the movement is a displacement of the stem relative to the head and stalk.

Stem and head are connected by a linker domain

Clues to the mechanism producing these changes arise from an analysis of rare, longer-stemmed dynein c molecules (Fig. 1, asterisk). Analysis revealed no consistent differences between ADP•Vi- and apo-molecules in this small data set, so we combined the images to improve the signal to noise ratio. Despite their structural heterogeneity, averages reveal several important features of the organization of the molecule (Fig. 2i–k). There is often a sharp, approximately 90° bend in the stem, at a position corre-
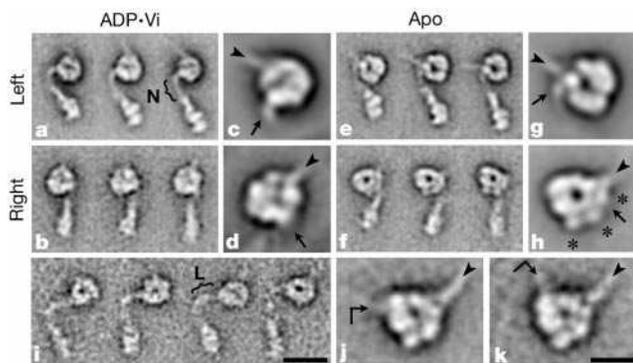
Figure 2 Characteristic views of dynein c revealed by single-particle analysis. Images are selected class averages of the most common views. **a–d**, ADP•Vi-dynein in left views (**a**) and right views (**b**); after head alignment in left view (**c**) and right view (**d**). **e–h**, Apo-dynein c in left views (**e**) and right views (**f**); after head alignment in left view (**g**) and right view (**h**). **i–k**, Selected class averages of rare molecules showing the linker (L) (**i**) and head substructure after head alignment (**j**, **k**). The location of stalk (arrowheads) and apparent stem attachment (arrows) on the head are indicated. N indicates the neck; asterisks indicate three subdomains. Left views represent about 50% of ADP•Vi- and apo-molecules; right views about 12%. Rare molecules represent about 6% of ADP•Vi- and apo-molecules. The numbers of images in each class average in **a**, **b**, **e** and **f** vary between 20 and 43, and in **i** between 5 and 6. The number of images in averages after head alignment are: **c**, 1,733; **d**, 361; **g**, 1,658; **h**, 346; **j**, 38 (18 ADP•Vi + 20 apo); and **k**, 23 (12 ADP•Vi + 11 apo). Scale bars: **a**, **b**, **e**, **f**, **i**, 25 nm; **c**, **d**, **g**, **h**, **j**, **k**, 10 nm.
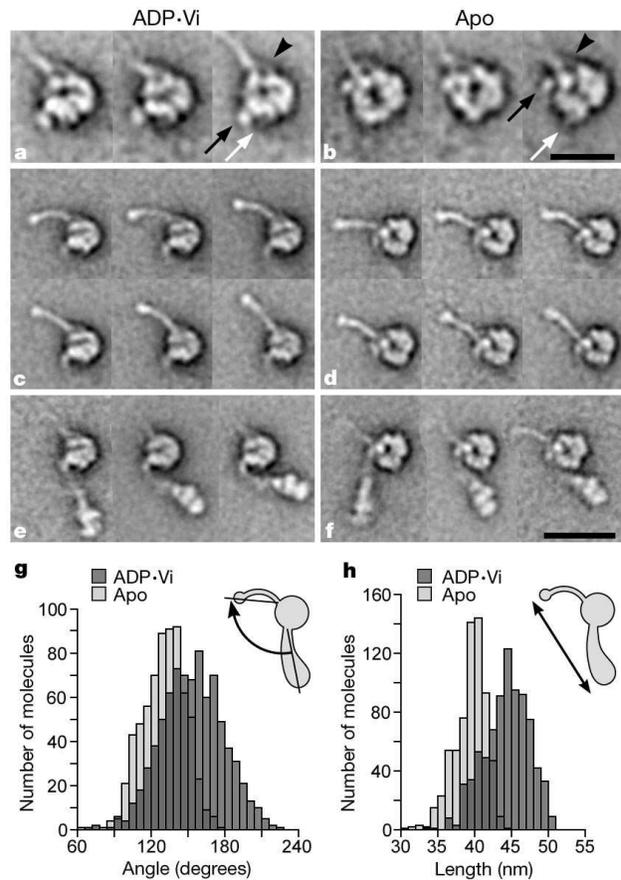
Figure 3 Substructure and flexibility within left views of dynein c. Head-aligned molecules (that is, those contributing to Fig. 2c, g) were further classified independently according to their heads, stalks and stems, using masks to isolate these structures. **a–f**, Image averages of selected classes of: ADP•Vi heads (**a**), apo-heads (**b**), ADP•Vi stalks (**c**), apo-stalks (**d**), ADP•Vi stems (**e**) and apo-stems (**f**). **a**, **b**, The stalk bifurcates near its point of attachment to the head (arrowheads). A fine structure emerges from the head (white arrows). The emergence point of the stem is indicated (black arrows). The number of images in class averages vary between 14 and 44. **g**, Distribution of stem–stalk angles. **h**, Distribution of molecular lengths. Scale bars: **a**, **b**, 15 nm; **c–f**, 25 nm.

sponding to the bend seen in the neck of typical molecules. Between this bend and the head is a hitherto unseen structure, similar in width to the neck and about 10 nm long, which we call the linker (Fig. 2i). Thus the stem consists of three distinct domains: base, neck and linker. The similarity of the head (Fig. 2j, k) to right views of typical apo-heads (Fig. 2h) shows that the head adopts the same orientation. However, the linker emerges from the left side of the head, diametrically opposite where the neck typically emerges (compare Fig. 2j, k to h; see also Supplementary movies 5 and 6). The straightforward interpretation is that the linker is normally docked onto one face of the head but in these rare molecules it is undocked, revealing the true site of insertion of the stem into the head. The docked linker lies across the upper face in right views, as the lower face, which is embedded in stain, appears unaffected by dissociation of the linker. Consistent with this, the neck is poorly defined in right views of typical molecules, indicating that it lies sufficiently far above the carbon substrate that it is above the stain. Thus movement of the docked stem between the ADP•Vi- and apo-conformations implies a swinging movement of the linker across the head.

Conformational changes in the stalk

The transition between ADP•Vi states and apo-states also causes structural changes in the stalk. This structure is revealed optimally by image classification of left views after head alignment to bring the bases of the stalks into register (Fig. 3c, d). The stalk is uniformly narrow (about 2 nm), except for a distinct enlargement at its tip. Where it joins the head (Fig. 3a, b, arrowheads), the stalk is resolved into two separate strands. These observations are compatible with other evidence that the stalk consists of two α-helices interacting as an anti-parallel coiled-coil, with the ATP-sensitive microtubule-binding domain at the tip[11,14–16,32]. Flexibility of the stalk produces a continuous range of conformations in both biochemical states, but the distribution of stalk chord angles indicates that the extent of flexibility is altered by loss of products. The standard deviation of the distribution (measured relative to the head) changes from 20° in ADP•Vi molecules ($n = 908$) to 11° in apo-molecules ($n = 721$),

indicating a stiffening of the stalk in apo-molecules. This is due, at least in part, to a structural change within the stalk, as ADP•Vi stalks are gently curved when flexed (that is, pointing leftwards; Fig. 3c, upper row) and straight when extended (pointing upwards; Fig. 3c, lower row), whereas apo-stalks (Fig. 3d) are always straight except for a slight kink about 5 nm from the tip (see Supplementary movies 1 and 2).

Power stroke of dynein

The conformational change seen in left views alters the angle between stem and stalk, and changes the overall length of the molecule. The mean angle between stem and stalk (Fig. 3g) decreases from 160° (ADP•Vi) to 136° (apo). The decrease in standard deviation of this distribution, from 25° (ADP•Vi) to 17° (apo) is accounted for by the stiffening of the stalk described above. There is no correlation between the angles of stem and stalk in individual molecules (data not shown), indicating that their movements are not coupled. The mean length of dynein c decreases markedly from 45.3 to 40.4 nm (Fig. 3h), producing the more compact apo-molecule apparent in raw images.

To examine the magnitude of the power stroke we compared images of left views showing the mean conformation of stem and stalk in ADP•Vi- and apo-molecules (Fig. 4a). Alignment of their stems suggests a mean displacement of 15 nm of the tip of the stalk (see Supplementary movie 7). A change in head orientation may also contribute to the apparent (projected) size of this displacement. This power stroke is longer than the 8-nm steps seen under load in optical trap experiments[30] that reflect the spacing of successive binding sites on the microtubule. Moreover, the flexibility of both neck and stalk implies that power stroke amplitudes can cover a wide range around this mean.

Discussion

How might these new structural data be reconciled with earlier findings? The appearance of the head of dynein c supports the idea of a toroidal arrangement of domains suggested previously[12,13,21,33]. The head is also large enough to accommodate at least six AAA domains arranged in a planar ring, as described by a hypothetical atomic model of dynein[33]. However, this model predicts a similar appearance of the two faces and six-fold rotational symmetry—neither is seen in our images. A possible origin of these discrepancies is that a seventh AAA module[34] and the C-terminal sequence[12] may contribute additional domains within the head. Furthermore, by lying across one face of the head, the linker would make the two faces appear different. Undocking of the linker from the head may explain two previous observations. First, images showing that the stem but not the stalk elongates when additional tension is applied to the multimeric outer-arm complex[9] can now be interpreted as domain movements within individual dynein heavy chains. Second, isolated molecules of other dynein species[9–11] display a structural heterogeneity and unexpected length similar to the rare undocked molecules of dynein c, suggesting that the linker has a weaker association in these species.

It has been proposed that stem, stalk or both act as mechanical levers, amplifying conformational changes originating within the head[12,13,15,21,32]. Our data show that amplification is achieved primarily through a change in head–stem orientation. This refines the conclusion from earlier studies on multimeric flagellar outer-arm dynein complexes *in situ*[11,28]. Flexibility in the stalk and neck suggest that these may be important compliant, although inextensible, linkages that are capable of storing elastic strain energy when the molecule develops force against a load. This ability may underlie the ATP-induced propagation of a zone of activity along isolated groups of flagellar microtubules[3]. Stiffening of the apo-stalk is compatible with the increased stiffness of nucleotide-free flagella over those bathed in ATP and vanadate[35]. The affinity of the microtubule-binding domain for its track is higher in apo-dynein than in
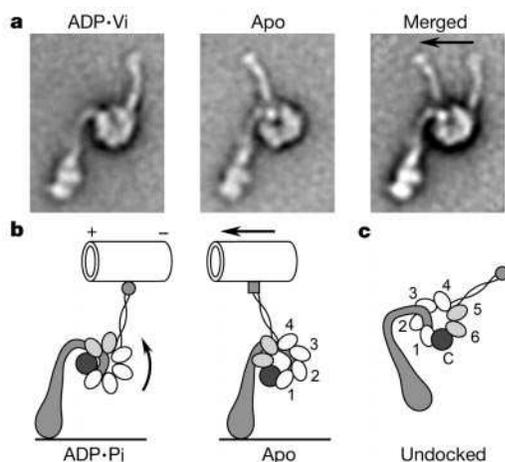
Figure 4 Structure and power stroke of dynein c. **a**, Left views of dynein c showing the mean conformation of the stem and stalk relative to the head. Images were made by compositing class averages having the mean stem and stalk angles. Images are shown after alignment of their stems. The arrow indicates 15 nm. **b**, Speculative structure of the molecule suggesting an origin of the power stroke and how this might be converted into microtubule movement. The six AAA modules (1–6) and C-terminal sequence (C) are indicated. The microtubule track (not drawn to scale) is illustrated as moving under zero load with its plus end leading[30]. **c**, Molecule showing the stem undocked from the head, shown as a right view for comparison with Fig. 2i–k. The same stem structure has been used in all illustrations.

 717

ADP•Vi-dynein[36], and microtubules activate the ATPase[37], implying two-way communication between the tip of the stalk and the ATPase site in the head[14,32]. Our finding that the conformation of the stalk itself changes indicates that this mechanism involves modifications in the structure of the coiled-coil.

We suggest a new model for the structure and mechanism of dynein c (Fig. 4b). Six AAA domains and a C-terminal domain form a planar ring[12], with the stalk emerging between AAA4 and -5, and a hook-shaped stem joining AAA1. The rare undocked appearance (Fig. 2i–k) can be understood as arising from a change in structure at the junction between the linker and AAA1, accompanied by undocking of the linker from the head. In molecules adsorbed to the carbon in the right view this allows the entire stem to flip over (Fig. 4c). The possible physiological relevance of such molecules is currently unknown. In the typical ADP•Vi molecule (Fig. 4b, left), the docked linker occludes the central channel and the stem emerges from the head far from the stalk. Microtubule movement is initiated by tight binding to the tip of the stalk, which promotes a concerted conformational change in AAA1–4, thereby activating release of ADP and phosphate from AAA1, the probable site of ATP hydrolysis[33]. Rigid coupling between AAA1 and linker causes a rolling of the head towards the stem, which translates the microtubule by 15 nm under zero load conditions. The resulting movement of AAA2–4 towards the linker increases the prominence of the central channel (Fig. 4b, right). Movement between AAA4 and -5 increases stalk stiffness by changing the structure of its junction with them. The approach of the apo-linker to this region may also be involved. Presumably, ATP binding to AAA1 reduces the microtubule-binding affinity without a complete reversal of this sequence of events. In support of the mechanism, both ATP and ADP binding within AAA1–4 (ref. 22) is required for optimal dynein function[24]. Nucleotide in these sites might favour conformational switching on the communication pathway. This mechanism offers the intriguing possibility that functionally significant interactions between AAA2–4 and the linker may occur, and be modulated by nucleotide. Our results identify that a change in head–linker orientation is fundamental in the power stroke of dynein.   □

Methods

Dynein c was purified from *C. reinhardtii* as described[30], except that to improve the quality of negative staining, the elution buffer for the final anion exchange column was a KCl gradient in 30 mM MOPS, 5 mM $MgCl_2$, 1 mM EGTA and 0.1 mM dithiothreitol, pH 7.4 (MMED buffer). Stock dynein samples (approximately 0.65 µM protein and about 200 mM KCl) were diluted 40-fold into MMED buffer containing 200 mM KCl. To generate ADP•Vi molecules, 100 µM ATP and 50 µM sodium orthovanadate were added at 4 °C for 30 min[38]. The specimen was applied to carbon grids treated with ultraviolet light, as described[39]. Before staining with 1% uranyl acetate[39], grids were rinsed with MMED buffer without KCl to improve staining. Micrographs were taken at a nominal magnification of × 40,000 and calibrated using the paramyosin spacing of 14.4 nm[40]. A total of 4,900 ADP•Vi molecules and 3,057 apo-molecules were selected interactively and subjected to single-particle image processing using procedures written in the SPIDER suite of programs[31]. Images were aligned by reference-free algorithms and classified into homogeneous groups by *K*-means clustering, as described[41]. Length and angle measurements were made from class averages and weighted according to the number of constituent images before calculating mean and standard deviation. *n* values are given as the total number of images, rather than classes.

1. Gibbons, I. R. Dynein family of motor proteins: present status and future questions. *Cell Motil. Cytoskel.* **32,** 136–144 (1995).
2. Gibbons, I. R. & Rowe, A. Dynein: a protein with adenosine triphosphatase activity from cilia. *Science* **149,** 424–426 (1965).
3. Vernon, G. G. & Woolley, D. M. The propagation of a zone of activation along groups of flagellar doublet microtubules. *Exp. Cell Res.* **220,** 482–494 (1995).
4. Woolley, D. M. The molecular motors of cilia and flagella. *Essays Biochem.* **35,** 103–115 (2000).
5. DiBella, L. M. & King, S. M. Dynein motors of the *Chlamydomonas* flagellum. *Int. Rev. Cytol.* **210,** 227–268 (2001).
6. Karki, S. & Holzbaur, L. F. Cytoplasmic dynein and dynactin in cell division and intracellular transport. *Curr. Opin. Cell Biol.* **11,** 45–53 (1999).
7. King, S. M. The dynein microtubule motor. *Biochim. Biophys. Acta* **1496,** 60–75 (2000).
8. Koonce, M. P. & Samso, M. Overexpression of cytoplasmic dynein's globular head causes a collapse of the interphase microtubule network in *Dictyostelium*. *Mol. Biol. Cell* **7,** 935–948 (1996).
9. Goodenough, U. W. & Heuser, J. Structural comparison of purified dynein proteins with *in situ* dynein arms. *J. Mol. Biol.* **180,** 1083–1118 (1984).
10. Goodenough, U. W. *et al.* High-pressure liquid chromatography fractionation of *Chlamydomonas* dynein extracts and characterization of inner-arm dynein subunits. *J. Mol. Biol.* **194,** 481–494 (1987).
11. Goodenough, U. W. & Heuser, J. E. in *Cell Movement: the Dynein ATPases* Vol. 1 (eds Warner, F. D., Satir, P. & Gibbons, I. R.) 121–140 (Alan Liss, New York, 1989).
12. King, S. M. AAA domains and organization of the dynein motor unit. *J. Cell Sci.* **113,** 2521–2526 (2000).
13. Asai, D. J. & Koonce, M. P. The dynein heavy chain: structure, mechanics and evolution. *Trends Cell Biol.* **11,** 196–202 (2001).
14. Gee, M. A., Heuser, J. E. & Vallee, R. B. An extended microtubule-binding structure within the dynein motor domain. *Nature* **390,** 636–639 (1997).
15. Vallee, R. B. & Gee, M. A. Make room for dynein. *Trends Cell Biol.* **8,** 490–494 (1998).
16. Koonce, M. P. & Tikhonenko, I. Functional elements within the dynein microtubule-binding domain. *Mol. Biol. Cell* **11,** 523–529 (2000).
17. Samsó, M., Radermacher, M., Frank, J. & Koonce, M. P. Structural characterization of a dynein motor domain. *J. Mol. Biol.* **276,** 927–937 (1998).
18. Gibbons, I. R., Gibbons, B. H., Mocz, G. & Asai, D. Multiple nucleotide-binding sites in the sequence of dynein β heavy chain. *Nature* **352,** 640–643 (1991).
19. Ogawa, K. Four ATP-binding sites in the midregion of the β heavy chain of dynein. *Nature* **352,** 643–645 (1991).
20. Neuwald, A. F., Aravind, L., Spouge, J. L. & Koonin, E. V. AAA + : a class of chaperone-like ATPases associated with the assembly, operation, and disassembly of protein complexes. *Genome Res.* **9,** 27–43 (1999).
21. Vale, R. D. AAA proteins: lords of the ring. *J. Cell Biol.* **150,** F13–F19 (2000).
22. Mocz, G. & Gibbons, I. R. Phase partition analysis of nucleotide binding to axonemal dynein. *Biochemistry* **35,** 9204–9211 (1996).
23. Gibbons, I. R. *et al.* Photosensitized cleavage of dynein heavy chains. *J. Biol. Chem.* **262,** 2780–2786 (1987).
24. Yagi, T. ADP-dependent microtubule translocation by flagellar inner-arm dyneins. *Cell Struct. Funct.* **25,** 263–267 (2000).
25. Shiroguchi, K. & Toyoshima, Y. Regulation of monomeric dynein activity by ATP and ADP concentrations. *Cell Motil. Cytoskel.* **49,** 189–199 (2001).
26. Johnson, K. A. Pathway of the microtubule-dynein ATPase and the structure of dynein: a comparison with actomyosin. *Annu. Rev. Biophys. Biophys. Chem.* **14,** 161–188 (1985).
27. Goodenough, U. W. & Heuser, J. E. Substructure of the outer dynein arm. *J. Cell Biol.* **95,** 798–815 (1982).
28. Burgess, S. A. Rigor and relaxed outer dynein arms in replicas of cryofixed motile flagella. *J. Mol. Biol.* **250,** 52–63 (1995).
29. Vale, R. D. & Milligan, R. A. The way things move: looking under the hood at molecular motor proteins. *Science* **288,** 88–95 (2000).
30. Sakakibara, H., Kojima, H., Sakai, Y., Katayama, E. & Oiwa, K. Inner-arm dynein c of *Chlamydomonas* flagella is a single-headed processive motor. *Nature* **400,** 586–590 (1999).
31. Frank, J. *Three-dimensional Electron Microscopy of Macromolecular Assemblies* (Academic, New York, 1996).
32. Gee, M. A. & Vallee, R. B. The role of the dynein stalk in cytoplasmic and flagellar motility. *Eur. Biophys. J.* **27,** 466–473 (1998).
33. Mocz, G. & Gibbons, I. R. Model of the motor component of dynein heavy chain based on homology to the AAA family of oligomeric ATPases. *Structure* **9,** 93–103 (2001).
34. Fan, J. & Amos, L. A. Antibodies to cytoplasmic dynein heavy chain map the surface and inhibit motility. *J. Mol. Biol.* **307,** 1317–1327 (2001).
35. Okuno, M. Inhibition and relaxation of sea urchin sperm flagella. *J. Cell Biol.* **85,** 712–725 (1980).
36. Vale, R. D., Soll, D. R. & Gibbons, I. R. One-dimensional diffusion of microtubules bound to flagellar dynein. *Cell* **59,** 915–925 (1989).
37. Omoto, C. K. & Johnson, K. Activation of the dynein adenosine triphosphatase by microtubules. *Biochemistry* **25,** 419–427 (1986).
38. Gibbons, I. R. & Mocz, G. Photocatalytic cleavage of proteins with vanadate and other transition metal complexes. *Methods Enzymol.* **196,** 428–442 (1991).
39. Walker, M. L. *et al.* Two-headed binding of a processive myosin to F-actin. *Nature* **405,** 804–807 (2000).
40. Elliot, A., Offer, G. & Burridge, K. Electron microscopy of myosin molecules from muscle and non-muscle sources. *Proc. R. Soc. Lond. B* **193,** 45–53 (1976).
41. Burgess, S. A., Walker, M. L., White, H. D. & Trinick, J. Flexibility within myosin heads revealed by negative stain and single-particle analysis. *J. Cell Biol.* **139,** 675–681 (1997).

Competing interests statement The authors declare that they have no competing financial interests.

Correspondence and requests for materials should be addressed to S.A.B. (e-mail: s.a.burgess@leeds.ac.uk).